International Conference on Mathematics, Computational Methods & Reactor Physics (M&C 2009)
Saratoga Springs, New York, May 3-7, 2009, on CD-ROM, American Nuclear Society, LaGrange Park, IL (2009)

MULTI-GROUP TRANSPORT METHODS FOR HIGH-RESOLUTION NEUTRON ACTIVATION ANALYSIS

Kimberly A. Burns, L. Eric Smith, Christopher J. Gesh, and Mark W. Shaver
Pacific Northwest National Laboratory
National Security Division, MS K8-34
Richland, WA 99352
kimberly.burns@pnl.gov; eric.smith@pnl.gov; gesh@pnl.gov; mark.shaver@pnl.gov

ABSTRACT

The accurate and efficient simulation of coupled neutron-photon problems is necessary for several important radiation detection applications. Examples include the detection of nuclear threats concealed in cargo containers and prompt gamma neutron activation analysis for nondestructive determination of elemental composition of unknown samples. In these applications, high-resolution gamma-ray spectrometers are used to preserve as much information as possible about the emitted photon flux, which consists of both continuum and characteristic gamma rays with discrete energies. Monte Carlo transport is the most commonly used modeling tool for this type of problem, but computational times for many problems can be prohibitive. This work explores the use of multi-group deterministic methods for the simulation of neutron activation problems.

Central to this work is the development of a method for generating multi-group neutron-photon cross-sections in a way that separates the discrete and continuum photon emissions so that the key signatures in neutron activation analysis (i.e., the characteristic line energies) are preserved. The mechanics of the cross-section preparation method are described and contrasted with standard neutron-gamma cross-section sets. These custom cross-sections are then applied to several benchmark problems. Multi-group results for neutron and photon flux are compared to MCNP results. Finally, calculated responses of high-resolution spectrometers are compared. Preliminary findings show promising results when compared to MCNP. A detailed discussion of the potential benefits and shortcomings of the multi-group-based approach, in terms of accuracy, and computational efficiency, is provided.

Key Words: Coupled Neutron-Photon Transport, Neutron Activation Analysis, Multi-Group Cross Sections, Neutron Photon Problems

1. INTRODUCTION

Neutron-induced photon signatures are an important component of many radiation detection and nondestructive assay (NDA) scenarios. One example is the screening of vehicles and cargo at border crossings wherein neutron-emitting threat sources (e.g. plutonium) can induce photon emissions in the surrounding cargo. Another familiar example is Prompt Gamma Neutron Activation Analysis (PGNAA), a technique used to determine the composition of unknown samples. In PGNAA, the sample is irradiated with a neutron source and the subsequent interactions in the material produce photons through a number of reactions, including inelastic scatter and radiative capture. The discrete-energy emissions represent (generally) unique fingerprints of isotopes in the sample, for example, the 2.223 MeV gamma ray produced from radiative capture in ^{1}H. The presence and relative portions of these discrete gamma rays can be

used to infer the chemical composition of the material being interrogated. In order to obtain the level of detail required to detect and quantify the key characteristic gamma rays, and thus determine elemental composition, the use of a high-resolution gamma-ray spectroscopy system is required.

At present, Monte Carlo is the primary tool for simulating neutron activation analysis problems, largely because it is able to preserve the important discrete-energy signatures throughout the problem. This culminates in a pulse-height tally in the high-resolution gamma-ray spectrometer. However, neutron-photons problems in Monte Carlo often require very long run times due to the high degree of scatter and absorption during neutron and photon transport.

Multi-group deterministic methods offer potential advantages for neutron-photon problems: an "infinite real measurement time" once convergence is reached and reduced computational times, most notably in problems with highly scattering or highly absorbing materials. The purpose of this research is to explore the use of multi-group deterministic methods for the simulation of coupled neutron-photon problems.

The work described here utilizes the RAdiation Detection Scenario Analysis Toolbox (RADSAT), a code which couples deterministic and Monte Carlo transport to perform radiation detection scenario analysis in three dimensions [1]. RADSAT is a collaboration between Pacific Northwest National Laboratory and Transpire, Inc. The deterministic core of RADSAT is Attila, a code originally developed by Los Alamos National Laboratory, and since expanded and refined by Transpire, Inc. [2]. Attila solves the transport equation on unstructured tetrahedral meshes, and it incorporates ray-effect mitigation techniques well-suited to radiation detection problems. MCNP5 is used for the calculation of detector response. Previous publications have described the use of RADSAT for photon-only transport problems [1][3], including the use of an adaptive energy group structure that preserves the discrete nature of characteristic gamma-ray emissions.

A major challenge in utilizing multi-group transport methods for neutron-photon problems is maintaining the neutron induced photon signatures throughout the problem. The preparation of suitable multi-group cross-sections is required in order to complete this task. We first describe the standard method for producing multi-group cross-sections, and why that is unsuitable for the simulation of high-resolution neutron activation analysis. We then describe our own method for preparing (n,γ) cross-sections, "RADSAT-NG", and provide comparisons with existing cross section sets. Next, we define a simple benchmark problem geometry that consists of a ^{252}Cf neutron source irradiating a cubical sample and a high-resolution gamma-ray spectrometer. Comparisons of the multi-group deterministic and Monte Carlo neutron-induced photon production rates are provided. Finally, a high-purity gamma-ray spectrometer response is calculated using MCNP5 [4] and RADSAT. We then discuss the strengths and limitations of the RADSAT method as compared to Monte Carlo only approaches, particularly in regard to pulse height spectra, the most important observable in radiation detection scenarios: the spectrometer pulse-height tally.

2. METHODS DISCUSSION

Our approach for simulating coupled neutron-photon problems consists of four steps:

1) A multigroup, deterministic neutron transport calculation of the source neutrons to all parts of the problem;
2) The generation of the corresponding spatially dependent neutron-induced gamma-ray spectrum;
3) A multigroup, deterministic photon transport calculation of the induced gamma-ray spectrum to all parts of the problem;
4) The calculation of the detector response (i.e. pulse-height tally) in a spectrometer with MCNP5.

The process is outlined in Figure 1. A description of neutron transport problems can be found in reference [2]. Multi-group methods for photon transport to the detector location, and the calculation of the detector response are detailed in previous RADSAT publications [1][3]. Our primary focus is the second step—the calculation of the spatially dependent neutron-induced gamma-ray spectrum and the development of the corresponding RADSAT (n,γ) cross-section library (RADSAT-NG).

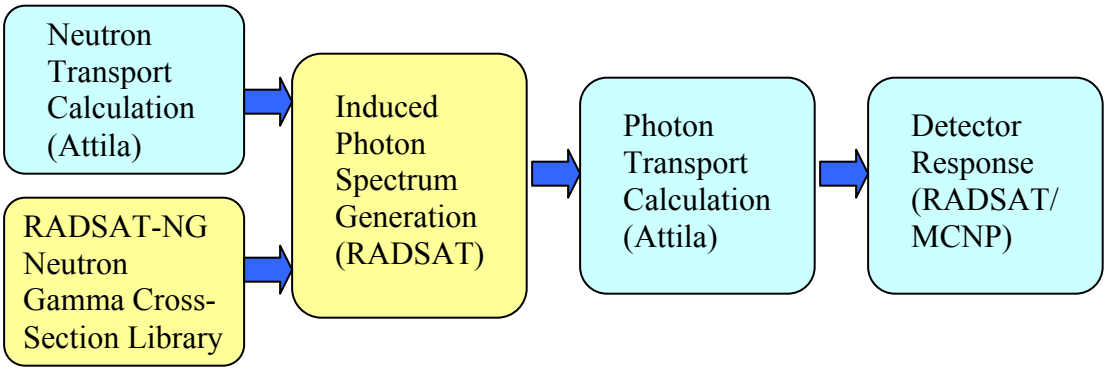

Figure 1. Procedure for Calculating Coupled Neutron-Photon Problems Using RADSAT. The yellow boxes (RADSAT-NG cross-section preparation and neutron-induced photon source generation using RADSAT) comprise the focus of this paper.

2.1. Neutron Transport Calculation

The neutron transport calculation was completed using Attila, the deterministic backbone of RADSAT [2]. All of the neutron transport calculations in this work were run with S_{16} Triangular Chebychev Legendre angular quadrature set, P_2 scattering moments, approximately 3000 spatial cells, and the Kynea3 cross section set [5]. The Kynea3 cross-section set was developed by Sandia National Laboratories and Oak Ridge National Laboratory as a general purpose library for radiation detection scenarios, and includes 36 energy groups below 5 eV, 25 energy groups from 5 eV to 1 MeV, and 18 energy groups above 1 MeV [5].

2.2. RADSAT-NG Neutron Gamma Cross-Section Library Preparation

Existing multigroup neutron gamma cross-section libraries, like those provided in the Attila distribution, are typically used for photon dose-rate and total flux calculations rather than high-

resolution gamma-ray spectroscopy. Consequently, existing cross-section libraries generally have relatively few (e.g. 10-20) broad photon groups spanning energies up to several MeV. They are unsuitable for the simulation of high-resolution gamma-ray spectroscopy which requires the preservation of discrete-energy photons. In addition, the existing coupled neutron-gamma cross-section libraries combine the cross-sections for discrete and continuum gamma productions into one multigroup gamma production matrix. This means that the production rate for the characteristic discrete-energy emissions—the key fingerprints in neutron activation analysis—cannot be calculated separately from the continuum. Instead, the discrete gamma-ray production rates are smeared into broad energy groups with the continuum.

As a first step, we explored the use of an existing cross-section preparation code that allows the user some flexibility in terms of energy group structure: the GROUPR subroutine of NJOY99 [6]. GROUPR can be used to generate multigroup cross-section libraries from ENDF/B data, with a neutron and photon energy group structure defined by the user. Unfortunately, GROUPR does not allow sufficient flexibility in photon group structure to achieve narrow energy bins about key discrete-energy emissions. Additionally, GROUPR does not differentiate between a discrete and continuum gamma ray produced by the same interaction. For these reasons, NJOY GROUPR was not able to produce suitable cross-section libraries for our work.

Therefore, to enable high-resolution multi-group neutron-photon analysis, we are developing a specialized cross-section set, RADSAT-NG. The unique feature of RADSAT-NG is that it supports the separate calculation of discrete and continuum photons, on a reaction-by-reaction basis, from a multigroup neutron flux. The partitioning of discrete and continuum photon production results in multigroup neutron cross-sections for the production of discrete gamma rays and a matrix of multigroup neutron photon cross-sections for the production of photons in the continuum. This separation allows the continuum cross-section to be expressed in coarse energy groups without the loss of spectral information and the discrete energy gamma rays to be produced and transported at their exact energy (or within a very narrow energy group), rather than smeared across a broad energy group preserving the spectral signatures in neutron activation analysis.

The preparation of RADSAT-NG cross-sections consists of 3 main steps:

1) Creation of point-wise cross-sections from the raw cross-section data in the ENDF/B format,
2) Application of Doppler broadening, as appropriate, and
3) Collapsing of point-wise data into a neutron-gamma production matrix with user-specified neutron and gamma energy group structures.

Steps 1) and 2) were performed using modules within NJOY99:

- RECONR module was used to reconstruct pointwise cross-sections from the resonance parameters and interpolation schemes in the ENDF/B format
- BROADR module was used to was used to calculate the Doppler broadening of the cross-sections
- ACER module was used to produce a point-wise cross-section file (of the form used by MCNP5).

The ACER module was key to the process because the file it produces contains separate cross-sections for the production of discrete gamma rays and for continuum photons. Both are

provided on a single union energy grid suitable for linear interpolation, making subsequent collapsing relatively straightforward.

Step 3), the collapsing of the point-wise cross-sections from the ACER files, was performed using software developed by PNNL, using conventional methods and common assumptions for the energy-dependent neutron and gamma flux weighting functions. [8] The point-wise cross-sections for the discrete gamma rays were collapsed into the neutron energy group structure of the Kynea3 cross-section library using Equation 1.

$$\sigma^{g}_{(n,\gamma\_discrete)} = \frac{\int_{E_g}^{E_{g-1}} dE_n \sigma_{(n,\gamma\_discrete)}(E_n \to E_\gamma)\varphi_n(E)}{\int_{E_g}^{E_{g-1}} dE_n \varphi_n(E)} \cong \frac{\sum_{E_g}^{E_{g-1}} \sigma_{(n,\gamma\_discrete)}(E_n \to E_\gamma)\omega_n(E)}{\sum_{E_g}^{E_{g-1}} \omega_n(E)} \tag{1}$$

where $\sigma_{(n,\gamma\_discrete)}(E_n \to E_\gamma)$ is the microscopic cross-section for a neutron with energy E_n to produce a discrete gamma ray with energy E_γ, $\varphi_n(E)$ is the neutron flux and ω_n is the neutron flux approximation. The continuum production was collapsed into the neutron-induced gamma production matrix using Equation 2.

$$\begin{aligned}\sigma^{g}_{(n,\gamma\_continuum)} &= \frac{\int_{E_g}^{E_{g-1}} dE_\gamma \int_{E_{g'}}^{E_{g'-1}} dE_n \sigma_{(n,\gamma\_continuum)}(E_n \to E_\gamma) p(E_n, E_\gamma)\varphi_n(E)\varphi_\gamma(E)}{\int_{E_g}^{E_{g-1}} dE_\gamma \int_{E_{g'}}^{E_{g'-1}} dE_n' \varphi_\gamma(E)\varphi_n(E)} \\ &\cong \frac{\sum_{E_g}^{E_{g-1}} \sum_{E_{g'}}^{E_{g'-1}} \sigma_{(n,\gamma\_continuum)}(E_n \to E_\gamma) p(E_n, E_\gamma)\omega_n(E)\omega_\gamma(E)}{\sum_{E_g}^{E_{g-1}} \sum_{E_{g'}}^{E_{g'-1}} \omega_n(E)\omega_\gamma(E)}\end{aligned} \tag{2}$$

$$\begin{aligned} \text{where}\quad \omega_n &= \exp(-E/1.025)\sinh\left(\sqrt{2.926E}\right) && 1x10^{-6}eV \le E_n < 100eV \\ \omega_n &= 1/E && 100eV \le E_n < 50keV \\ \omega_n &= \frac{2\pi}{(\pi kT)^{3/2}}\sqrt{E}\exp(-E/kT) && 50keV \le E_n \le 20MeV \\ \omega_\gamma &= 1 \end{aligned}$$

where $\sigma_{(n,\gamma\_continuum)}(E_n \to E_\gamma)$ is the microscopic cross-section for a neutron with energy E_n to produce a continuum gamma ray, $p(E_n,E_\gamma)$ is the probability that an incident neutron with energy E_n will produce a continuum gamma ray with energy E_γ, $\varphi_n(E)$ and $\varphi_\gamma(E)$ are the neutron and gamma flux, and ω_n and ω_γ are the neutron and gamma flux approximations, respectively. The neutron flux used for the collapsing was approximated as a Maxwellian in the thermal region, 1/E in the epithermal region, and a Watt-fission spectrum in the fast region [8]. The neutron flux approximation is accurate for the PGNAA application since the source typically used is a fission source such as a ^{252}Cf neutron source. The gamma-ray flux for the collapsing was approximated as uniform over the entire energy range since the continuum photon flux should not change significantly within a particular energy group. This assumption is supported by the facts that photon cross-sections above the x-ray absorption edges are smooth and without resonance

features and the continuum energy groups in RADSAT-NG are defined to be relatively narrow (generally less than 50 keV).

Ideally, the RADSAT-NG cross-sections would be benchmarked against existing cross-sections on a reaction-by-reaction, discrete-line by discrete-line basis. Lacking an equivalent line-by-line cross-section set, the basis for benchmarking of RADSAT-NG becomes a comparison to existing multi-group cross-section sets, using the sum over all reactions, and over all discrete and continuum photon production. A comparison of the multi-group radiative capture photon production cross-sections for ^{56}Fe, as produced by RATSAT-NG and the GROUPR subroutine of NJOY is shown in Figure 2. The two methods show good agreement in all non-resonance regions, but diverge in the resonance regions. While the RADSAT-NG and GROUPR resonance regions compared more favorably in many isotopes, the kind of discrepancies showed in Figure 2 are not uncommon. The reasons for these discrepancies are still under investigation, but they include different formulations for resonance self-shielding and in the background cross-section assumptions.

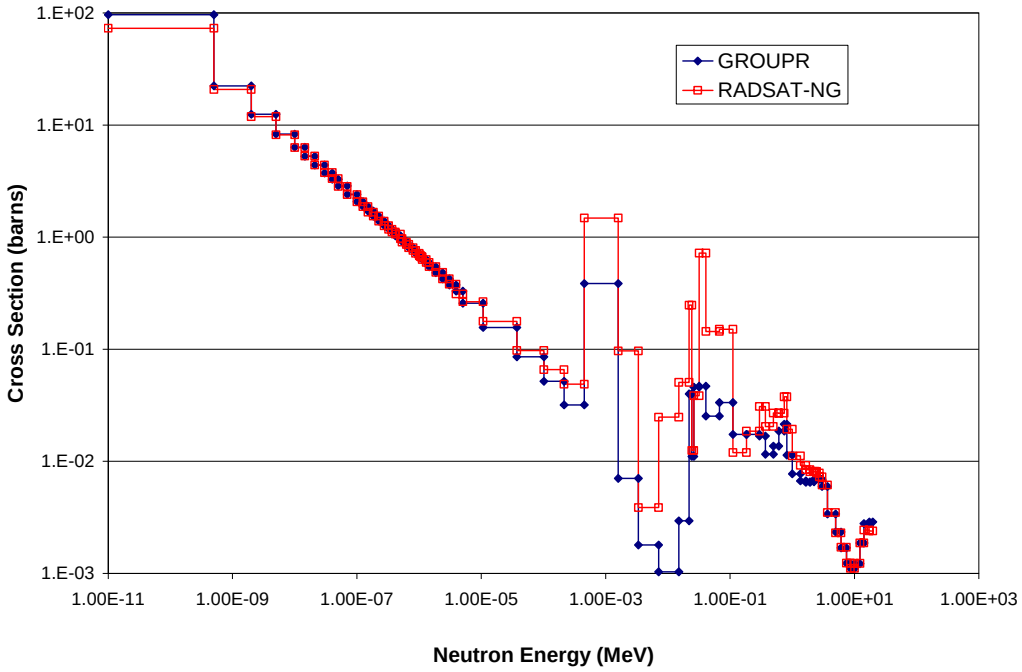

Figure 2. Radiative Capture Photon Production Cross-Section in ^{56}Fe, as calculated by RADSAT-NG and NJOY's GROUPR.

While the discrepancy in the resonance regions is unresolved, benchmarking calculations can help quantify the impact of those discrepancies on the results. For example, for isotopic cross-sections that have few resonance features, or the absolute magnitude of the resonance is low compared to other regions, there may have little or no impact. More discussion on this topic is provided in the Results and Conclusions sections.

2.3. Induced Photon Spectrum Generation

The calculation of the spatially dependent neutron-induced photon spectrum is completed by determining the photon production rate, $R(r,E_\gamma)$, as a function of position and gamma-ray energy as shown in Equation 3.

$$R(\vec{r}, E_\gamma) = N\sigma_{(n,\gamma)}(E_n \rightarrow E_\gamma)\varphi_n(E, \vec{r}) \quad (3)$$

where N is the number density, $\varphi_n(E,r)$ is the spatially dependent neutron flux, and $\sigma_{(n,\gamma)}(E_n \rightarrow E_\gamma)$ is the gamma production cross-section. The spatially dependent neutron flux was obtained from volume-averaged neutron flux edits in Attila. The RADSAT-NG cross-sections are then used for the gamma production cross-section. This reaction rate, and therefore photon production rate, is calculated on a volume-by-volume basis within the Attila problem. Various volume-partitioning schemes have been used to explore the effect of the neutron flux spatial variation on the fidelity of the photon production rate and energy spectrum.

2.4. Photon Transport Calculation

The energy- and position-dependent neutron-induced photon source term calculated in Equation 3 is then used as the photon source term in a photon transport calculation in RADSAT. The photon energy group structure for the gamma problem is defined using an adaptive approach described in detail in [1]. To preserve the important gamma-ray lines, narrow "peak" groups (typically 0.5 keV or less) are centered around the most prominent emission energies in the problem. All lower-yield discrete emissions, and any continuum source terms are then distributed into broader continuum groups that fill the energy range between peak groups.

Once the energy group structure is determined using this adaptive algorithm, the group structure is used to generate a problem-specific photon cross-section library using CEPXS [7]. The spatially dependent neutron-induced gamma spectrum and the photon cross-section library are then used in Attila to complete the photon transport to the detector location. RADSAT photon transport approaches are a combination of analytical ray-tracing, integral transport, and discrete ordinates methods—an approach capable of mitigating ray effects for many radiation-detection scenarios. The result of these calculations is a multigroup, discrete ordinates angular flux at all points in the problem. The angular flux can then be used for subsequent pulse height tally calculations at the detector location. All of the photon-only transport calculations in this work were run with S_{16} Triangular Chebychev Legendre angular quadrature set, P_5 scattering moment, and approximately 3000 spatial cells.

2.5. Gamma-Ray Spectrometer Response

The multi-group photon angular flux at the detector location is calculated in the photon transport and is used as the source term for a "near-field" Monte Carlo simulation for pulse-height tally in the gamma-ray spectrometer. The pulse-height tally is calculated using MCNP5 in this work, and recorded in uniform, narrow energy bins (typically 1 keV wide or less). A detailed explanation of the mechanics and utility of the RADSAT coupling method is provided in [3].

3. RESULTS AND DISCUSSION

With the goal of code-to-code verification for the RADSAT neutron-gamma methods, RADSAT results were compared to MCNP5 results for a series of simple neutron-activation benchmark problems. The geometric configuration for these problems is shown below in Figure 3 where a ^{252}Cf neutron source was placed 5 cm from one face of an 8000 cm^3 cube composed of various homogeneous materials. A coaxial high-purity germanium (HPGe) spectrometer, with a relative efficiency of 11% (active crystal dimensions approximately 5 cm in diameter by 3 cm thick, full-width at half-maximum energy resolution of approximately 3 keV at 1333 keV) was placed 2 cm away from the opposing face of the cube. Several material compositions, beginning with common single- and two-element materials with varying neutron-induced photon production behavior, were defined for testing. In this work, the results from cubes composed of nitrogen, iron and polyethylene are presented and discussed. The cube was further broken down into 64 sub-volumes so that spatial variation in the neutron flux characteristics, and the resulting photon production rates, could be accurately represented.

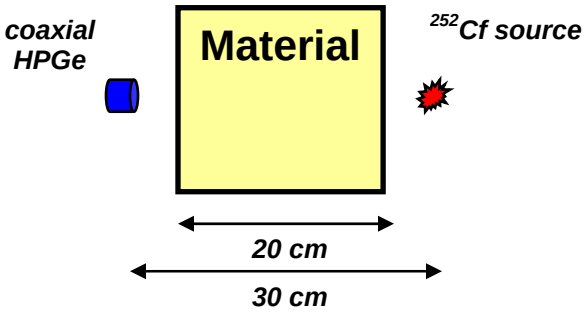

Figure 3. Source-sample-detector geometry for the neutron activation analysis problems used in code-to-code comparisons of RADSAT and MCNP5.

2.6. Nitrogen Test Case

Nitrogen represents a material of intermediate complexity in terms of coupled neutron-photon problems: ^{14}N has eight gamma producing reactions in the neutron energy range included in the Kynea3 neutron energy group structure (1e-5 eV to 19.64 MeV), but none of those reactions have strong resonances that might be difficult for the current RADSAT-NG library to model. There are a total of 136 discrete gamma rays and one continuum produced by neutron activation in ^{14}N. A comparison of the volume averaged photon flux, as tallied over the detector volume, for MCNP and RADSAT is shown in Figure 4.

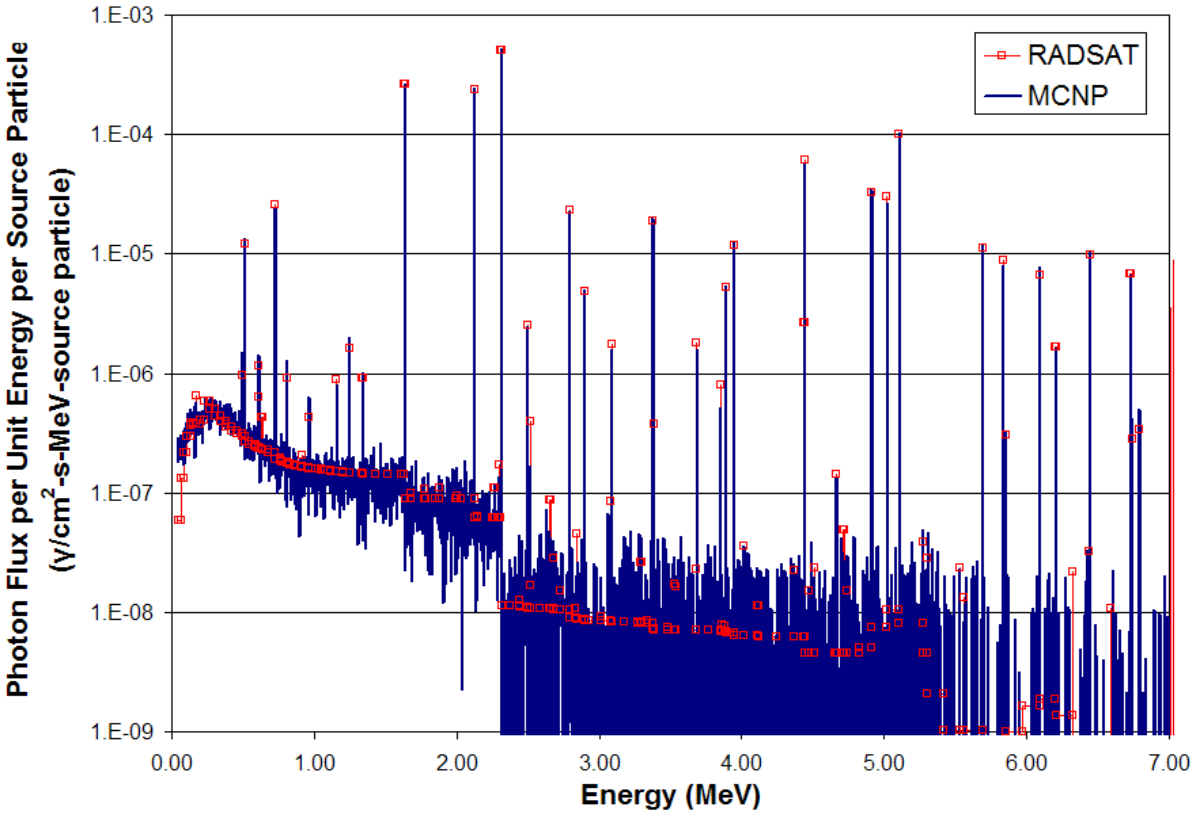

Figure 4. Code-to-code comparison using RADSAT and MCNP5 of volume averaged flux at the detector location for neutron activation analysis of nitrogen.

A comparison of the 5 highest intensity gamma rays for MCNP and RADSAT show typical agreement to within 3%, consistent with the statistical uncertainty of the MCNP calculation of 4% for the same lines. Larger discrepancies emerge between RADSAT and MCNP for lower-yield lines, but those are likely attributable to larger statistical uncertainties in the MCNP calculations.

2.7. Iron Test Case

Neutron activation in iron represents yet another step up in complexity, and is an important test case because it is a common material in many detector applications. The four naturally occurring iron isotopes, ^{54}Fe, ^{56}Fe, ^{57}Fe and ^{58}Fe, undergo 64 different photon-producing reactions which results in the production of 31 continua and 531 discrete gamma rays. Further, the resonance features in the iron cross-sections are significantly more complicated then those in nitrogen. The test-case sample volume was defined to use natural isotopic ratios: 5.845% ^{54}Fe, 91.754% ^{56}Fe, 2.119% ^{57}Fe, and 0.282% ^{58}Fe. A comparison of the volume-averaged photon flux at the detector location, for both MCNP and RADSAT calculations, is shown in Figure 5.

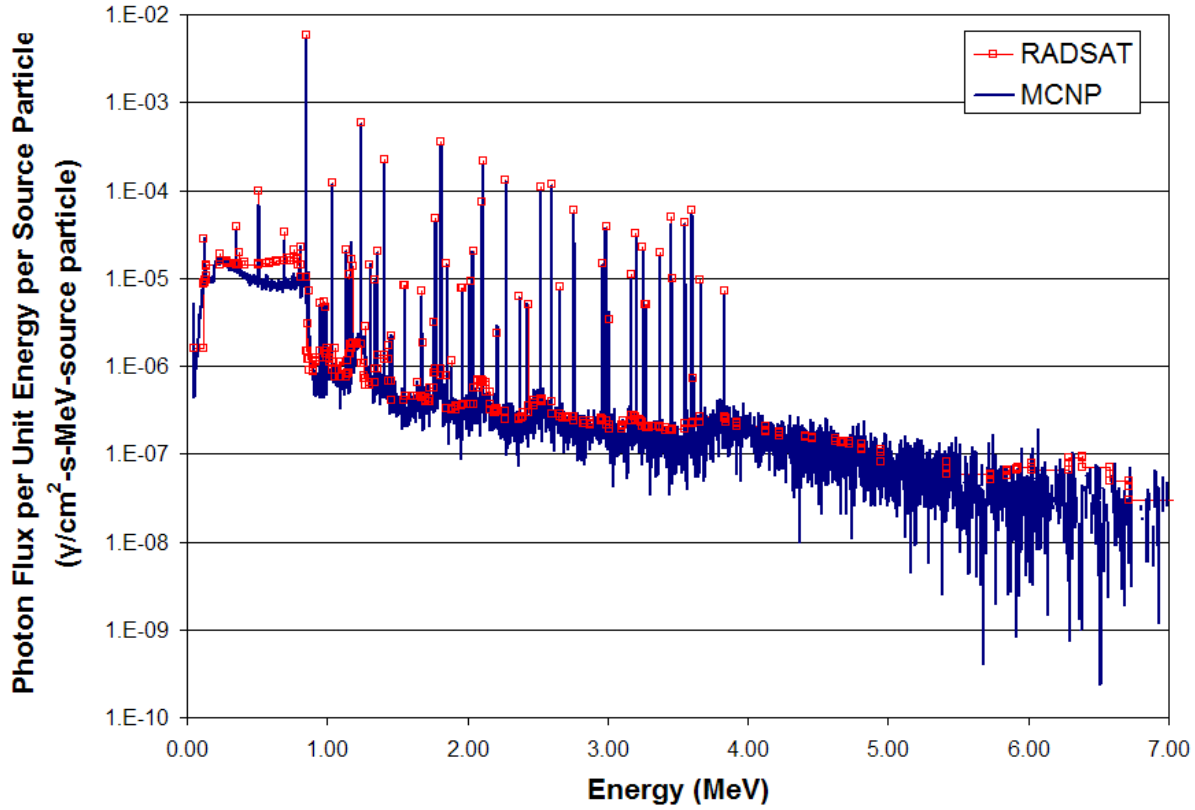

Figure 5. Code-to-code comparison using RADSAT and MCNP5 of volume averaged flux at the detector location for neutron activation analysis of iron.

As with the nitrogen test cases, the RADSAT and MCNP methods for iron are in agreement for both the continuum and discrete-line emissions. For the 5 most intense lines, RADSAT and MCNP differed by less than 1.5%; MCNP statistical variation for those same lines ranged from 1.2% to 6.1%. There is however, a notable discrepancy in the continuum immediately below the most intense gamma-ray emission in the problem at 0.849 MeV. The reason for this difference is still under investigation, but one possibility is an insufficient scattering order in the RADSAT photon-transport calculations (making it difficult to resolve the anisotropy in the low-angle scatter region).

2.8. Polyethylene Test Case

The polyethylene test case is the first two-element material used for the validation of RADSAT-NG cross-sections and RADSAT neutron activation methods. The polyethylene case is particularly useful because it allows a direct comparison of the photon production rates calculated with RADSAT and the neutron reaction rates obtained from MCNP (photon production rates cannot be tallied). This is possible because the C and H neutron-induced reactions produce only discrete gamma rays (no continuum photon production), and because the photon yield per neutron interaction is unity for the inelastic scatter and radiative capture reactions for carbon, hydrogen and deuterium. Those comparisons are shown in Table I for each reaction in the problem. The main source of discrepancies between the reaction rates obtained from MCNP and RADSAT is likely attributed to approximations used in the generation of

RADSAT-NG multigroup cross-sections, particularly the methods used in collapsing resonance regions (see Methods discussion). Unlike hydrogen, the photon production cross-section for inelastic scattering in carbon does have some contributions from resonances, which is supporting evidence for this claim. The larger discrepancies for the radiative capture photon production rate may be due to the presence of the cross-section above the energy range of the multi-group cross-section library.

Table I. ^{1}H, ^{2}H and ^{12}C Radiative Capture and Inelastic Scatter Reaction Rates

Nuclide	Reaction	RADSAT	MCNP	MCNP Relative Error	% Diff
^{1}H	Capture	4.82E-06	4.74E-06	0.0001	**1.68**
^{2}H	Capture	8.60E-13	8.49E-13	0.0001	**1.29**
^{12}C	Capture	2.34E-08	2.42E-08	0.0001	**3.31**
^{12}C	Scatter	1.83E-07	1.78E-07	0.0002	**2.81**
Total	---------	5.03E-06	4.94E-06	---------	**1.79**

A comparison of the volume-averaged photon flux at the detector location, using both MCNP and RADSAT, is shown graphically in Figure 6. That comparison indicates very good agreement in both the peak and continuum regions. A more quantitative comparison of the peak intensities is provided in Table II. The discrepancy between RADSAT and MCNP5 for the 6.25 MeV line is consistent with poor statistics in the Monte Carlo simulation.

Table II. Quantitative Peak Comparisons for Polyethylene Using MCNP and RADSAT.

	Discrete Gamma-Ray Energy (MeV)						
	1.2625	**2.223**	**3.684**	**4.439**	**4.9465**	**6.25**	**Total**
MCNP (γ/sec-cm^2)	2.88E-08	1.74E-05	2.99E-08	3.51E-07	6.57E-08	2.54E-12	2.35E-05
MCNP Error (%)	2.89	0.12	2.85	0.84	1.92	100	0.18
RADSAT (γ/sec-cm^2)	3.01E-08	1.88E-05	3.22E-08	4.01E-07	7.01E-08	3.46E-12	2.46E-05

Detector response calculations using RADSAT and MCNP for the neutron activation analysis of polyethylene were performed and are shown in Figure 7. Key observations from that comparison include the obscuring of the lower-energy, lower-yield 0.511 MeV annihilation line from the sample, but the enhancement of the double-escape peak at 1.20 MeV (due to relatively low stopping power, in the small HPGe spectrometer, for the 2.223 MeV line produced from ^{1}H radiative capture). The total count rate in the prominent peak regions agreed to within 5% for the RADSAT and MCNP5 calculations. The statistical uncertainty of the MCNP5 calculations varied from 3.9% in the region of the 1.2 MeV line to 27.7% in the region of the 3.9 MeV line.

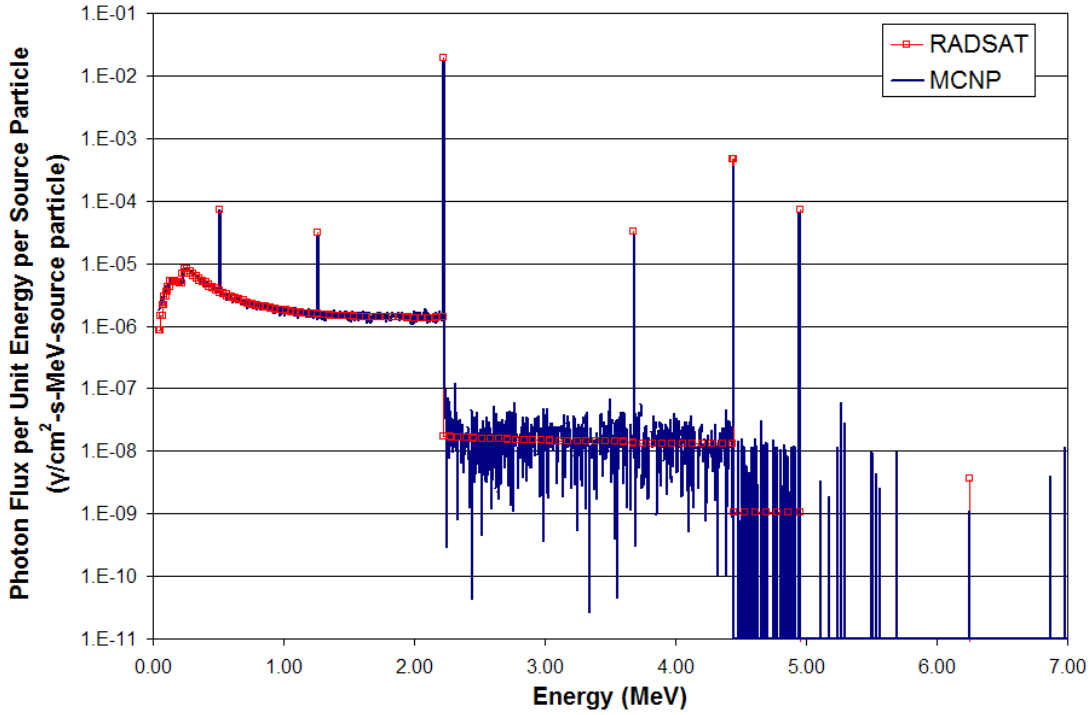

Figure 6. Code-to-code comparison using RADSAT and MCNP5 of volume averaged flux at the detector location for neutron activation analysis of polyethylene.

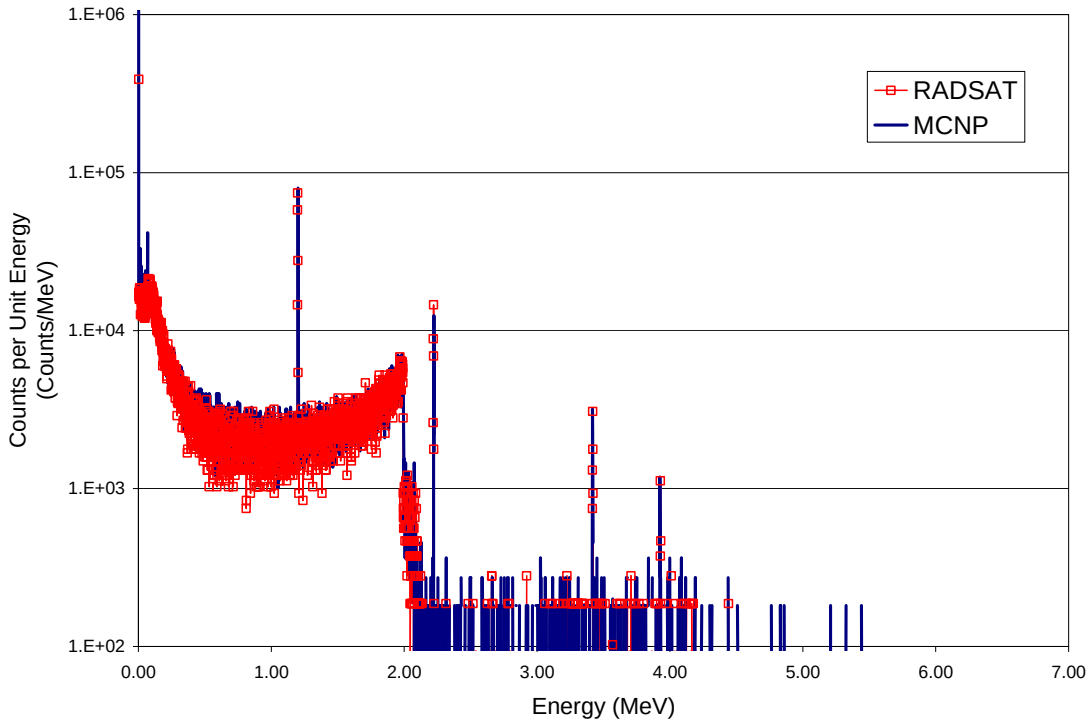

Figure 7. RADSAT and MCNP5 results for pulse-height tally in HPGe spectrometer viewing polyethylene sample.

4. CONCLUSIONS

Based on a series of simple benchmarking problems, and comparison to MCNP5 results, the deterministic transport methods being developed and implemented in RADSAT are capable of accurately and efficiently modeling neutron activation analysis problems utilizing high-resolution gamma-ray spectrometers. The key enabler for this functionality is the RADSAT-NG multi-group cross-section preparation method which, unlike currently available neutron-gamma cross-section libraries and preparation methods, tabulates the discrete-energy and continuum neutron-induced photon source terms separately. A series of simple benchmark problems showed good agreement between RADSAT- and MCNP-calculated photon production rates and photon transport to a detector location. The polyethylene test case demonstrated good agreement between RADSAT and MCNP for a pulse-height tally in a high-resolution HPGe spectrometer.

While demonstrating solution accuracy is the necessary first step in the use of RADSAT for neutron activation analysis problems, the primary motivator for using deterministic over Monte Carlo methods is the potential for significantly lower computational times that might enable new ways of approaching, for example, field analysis of PGNAA spectra recorded from unexploded chemical munitions. In this work, the RADSAT and MCNP5 computational times for each problem were recorded, and normalized to a typical single-processor 3 GHz desktop computer. For the series of test cases performed to date, the run times for RADSAT were approximately 10-1000 times shorter than for MCNP, when assuming a 40 mCi ^{252}Cf neutron source and 10 minutes of "real-world measurement time," values not atypical of PGNAA applications. For the neutron activation of polyethylene, MCNP required 4900 hours of computational time and RADSAT required 5 hours.

It is important to note, however, that these run-time comparisons can vary widely depending on the composition of materials in the problem, size of the problem, and the skill of the analyst in extracting the best performance from RADSAT and MCNP5. In this preliminary work, there was little effort to optimize the RADSAT calculational parameters in order to reduce run time; nor did we apply any substantive variance reduction methods (beyond geometry biasing on the neutron source) in the MCNP simulations. This work, therefore, represents only a preliminary assessment of RADSAT methods using a narrow subset of neutron activation problems. The results should not be interpreted to mean that the RADSAT-NG cross-section preparation methods are mature and well-vetted, or that RADSAT will always offer improved computational efficiency over Monte Carlo methods for neutron activation problems in general. Ongoing work, including more accurate treatment of resonance regions in the neutron-photon cross-section collapsing process, and additional evaluation of spatial discretization in the calculation of neutron flux and neutron-induced photon source terms, will shed more light on both aspects—accuracy and computational efficiency—and allow a more thorough evaluation of the strengths and limitations of RADSAT methods over a wide range of radiation detection problems.

ACKNOWLEDGMENTS

The authors would like to thank the National Nuclear Security Administration Office of Nonproliferation Research and Engineering (NA-22), for their support of RADSAT development. We are also grateful to Gus Caffrey of Idaho National Laboratory for his support of RADSAT as it might be applied in PGNAA for the assay of unexploded chemical munitions. The RADSAT team is also indebted to John Mattingly of Sandia National Laboratories for providing PNNL with the Kynea3 cross-section library. We would also like to thank Jeffery Favorite of Los Alamos National Laboratory for his work in converting the Kynea3 library to a format suitable for use in Attila. And finally, PNNL is highly appreciative of its RADSAT collaborators at Transpire, Inc., particularly Todd Wareing and Ian Davis, for their deterministic transport expertise.

REFERENCES

1. L.E. Smith, et al., "Coupling Deterministic and Monte Carlo transport Methods for the Simulation of Gamma-Ray Spectroscopy Scenarios," *IEEE Trans. Nucl. Sci.* (2008).
2. J.M. McGhee, et al., *Attila User's Manual*, Transpire, Inc. (2007).
3. M.W. Shaver, et al., "The Coupling of a Deterministic Transport Field Solution to a Monte Carlo Boundary Condition for the Simulation of Large Gamma-Ray Spectrometers," submitted to *Nuclear Technology* (2008).
4. *MCNP—A General Monte Carlo N-Particle Transport Code*, Los Alamos National Laboratory, LA-UR-03-1987 (2003).
5. E.S. Varley and J. Mattingly, "Rapid Feynman-Y Synthesis: Kynea3 Cross-Section Library Development," *Trans. Amer. Nucl. Soc.*, Vol. 98, pp.575 – 576 (2008).
6. *NJOY99.0 – Code System for Producing Pointwise and Multigroup Neutron and Photon Cross-Sections from ENDF/B Data,* Oak Ridge National Laboratory, PSR-480/NJOY99.0 (2000).
7. L.J. Lorence, "CEPXS/ONELD Version 2.0: A Discrete Ordinates Code Package for General One-Dimensional Coupled Electron-Photon Transport," *IEEE Trans. Nucl. Sci.*, 39, 1031, 1992.
8. J.J. Duderstadt and L.J. Hamilton, *Nuclear Reactor Analysis*, John Wiley & Sons, Inc., New York, USA (1976).